Applied Surface Science 450 (2018) 372–379

Contents lists available at ScienceDirect

Applied Surface Science

journal homepage: www.elsevier.com/locate/apsusc

Full Length Article

Effects of ambient humidity and temperature on the NO_2 sensing characteristics of WS_2/graphene aerogel

Wenjun Yan [a,b,c], Marcus A. Worsley [d], Thang Pham [e,f,g], Alex Zettl [e,f,g], Carlo Carraro [a,b], Roya Maboudian [a,b,*]

[a] Berkeley Sensor & Actuator Center, University of California, Berkeley, CA 94720, United States
[b] Department of Chemical and Biomolecular Engineering, University of California, Berkeley, CA 94720, United States
[c] Smart City Research Center of Zhejiang, Hangzhou Dianzi University, Hangzhou 310018, China
[d] Physical and Life Science Directorate, Lawrence Livermore National Laboratory, Livermore, CA 94550, United States
[e] Department of Physics, University of California, Berkeley, CA 94720, United States
[f] Materials Sciences Division, Lawrence Berkeley National Laboratory, Berkeley, CA 94720, United States
[g] Kavli Energy NanoSciences Institute at the University of California, Berkeley and the Lawrence Berkeley National Laboratory, Berkeley, CA 94720, United States

ARTICLE INFO

Article history:
Received 3 February 2018
Revised 7 April 2018
Accepted 20 April 2018
Available online 22 April 2018

Keywords:
WS_2/graphene aerogel
Heterojunction
NO_2 sensing
Humid air conditions

ABSTRACT

The effects of ambient humidity and temperature on the NO_2 sensing characteristics of WS_2/graphene aerogel (WS_2/GA) composite are investigated. In order to probe the gas sensing performances of WS_2/GA, the sensor is fabricated by integrating WS_2/GA with a microfabricated two-electrode device. The WS_2/GA is characterized by scanning electron microscopy (SEM), transmission electron microscopy (TEM), Raman spectroscopy, X-ray diffraction (XRD), X-ray photoelectron spectroscopy (XPS), and nitrogen porosimetry. This hybrid nanomaterial is found to improve the selectivity to NO_2, compared to control graphene and WS_2 aerogels. The NO_2 sensing performance of the WS_2/GA-based sensors is investigated under different relative humidities (0–60%), and ambient temperatures (room temperature (RT) to 180 °C). In all cases, the sensors exhibit p-type behavior. In dry atmosphere, faster response and better recovery are obtained with increasing temperature, reaching optimum sensing performance around 180 °C. At room temperature, interestingly, humidity is found helpful for enhancing the response and recovery of the sensor to NO_2. Detection limits in the range of 10–15 ppb NO_2 were determined. A possible gas sensing mechanism for this composite aerogel is proposed.

1. Introduction

Nitrogen dioxide (NO_2) gas is an increasing problem for air quality all over the world. The gas can cause serious problems such as lung damage, acid smog or rain. As little as 50 ppb can cause airway inflammation in lungs. Additionally, humidity is not a well-characterized parameter in practical environments. The detection of NO_2 at ppb-level concentrations in harsh environment (such as high humidity and high temperature) requires advances in sensing materials to provide the necessary performance characteristics. In previous reports, most NO_2 sensors working under high humidity were based on metal oxides [1–4] and yttria-stabilized zirconia (YSZ) [5,6]. For these sensors, the detection concentration of NO_2 was high (>1 ppm) [1,3], or the sensitivity to NO_2 decreased rapidly as the relative humidity of the atmosphere increased [4,7]. Therefore, significant work remains to develop high performance NO_2 sensors in various challenging environments.

The applications of graphene in a wide range of areas, including chemical sensing with low detection limits, have been explored due to its remarkable properties such as large surface area, excellent thermal conductivity, and high Young's modulus [8]. More recently, two-dimensional layered transition metal dichalcogenides (TMDCs), such as WS_2, are being explored as promising alternatives to graphene, because of their adjustable bandgap while exhibiting a high surface area [9]. The NO_2 sensing performance of WS_2 nanosheets has been reported recently [10]. Unfortunately, both graphene and WS_2-based sensors exhibit poor selectivity and incomplete recovery at room temperature [8,10–14], which limits their practical application. However, graphene with proper surface modification, including with TMDCs, can show great selectivity to various analyte gases [15,16]. An improved response/recovery rate and complete recovery can be attained by heating the sensing material [13,17]. Additionally,

* Corresponding author at: Berkeley Sensor & Actuator Center, University of California, Berkeley, CA 94720, United States; and Department of Chemical and Biomolecular Engineering, University of California, Berkeley, CA 94720, United States.
E-mail address: maboudia@berkeley.edu (R. Maboudian).

https://doi.org/10.1016/j.apsusc.2018.04.185
0169-4332/

limited reports on the NO_2-sensing characteristics of graphene in high humidity atmosphere are available [18–20].

In general, when a 2D layered sensing material is integrated into a device as a thin component, its surface area is limited by the device footprint. Assembling 2D sheets into 3D aerogel opens up a new way to enhance sensing performance by maintaining a high surface area in an open porous network [21–24]. Herein, the WS_2/graphene composite aerogel are synthesized and characterized. The effects of ambient humidity and temperature on the gas sensing properties of the composite aerogel are investigated in order to achieve an optimized NO_2 gas sensor working in a range of practical daily conditions.

2. Experimental

2.1. Synthesis and characterization methods

The WS_2/GA synthesis process is schematically shown in Fig. 1. High-quality graphene was synthesized according to our previous report [22]. Typically, 3 mL of an aqueous graphene oxide suspension (2 wt% graphene oxide) was mixed with 500 μL concentrated ammonium hydroxide (NH_4OH). The vial was sealed and placed in an oven at 85 °C for 12 h. The resulting wet gel was washed in deionized water to remove NH_4OH followed by an exchange of water with acetone inside the pores. Supercritical CO_2 was used to dry the gel, which was then converted to the graphene aerogel (GA) by pyrolysis at 1050 °C under nitrogen for 3 h. The GA was subjected to an additional thermal annealing at 2000 °C in He to improve the graphene crystallinity. For WS_2 coating, the GA was immersed in 1 mol/L ammonium thiomolybdate (ATT) solution and submerged in liquid nitrogen to rapidly freeze the solution. The frozen solution is then freeze-dried to produce an ATT-coated graphene aerogel. The ATT-coated graphene aerogel was annealed in 2% H_2/Ar mixture at 700 °C for 4 h to yield the WS_2/-graphene aerogel (WS_2/GA).

The morphology and structure of the WS_2/graphene aerogel are characterized using scanning electron microscopy (SEM, FEI Sirion XL30), transmission electron microscopy (TEM, JEOL 2010) and X-ray diffraction (XRD, AXS D8 Discover General Area Detector Diffraction System form Bruker with radiation from a Cu target, Kα, λ = 0.15406 nm). Raman spectroscopy (HORIBA Jobin Yvon LabRam spectrometer equipped with an Olympus microscope, and a 632.8 nm laser as the excitation source), and X-ray photoelectron spectroscopy (XPS, Omicron Dar400 system with an achromatic Al Kα X-ray source) are used for chemical and elemental analyses. Surface area properties are determined by Brunauer-Emmett-Teller (BET) and Barrett-Joyner-Halenda (BJH) methods using an ASAP 2020 surface area analyzer (Micromeritics Instrument Corporation) via nitrogen porosimetry. For the nitrogen porosimetry analyses, samples of approximately 0.1 g were heated to 150 °C under vacuum (10^{-5} Torr) for at least 24 h to remove all adsorbed species.

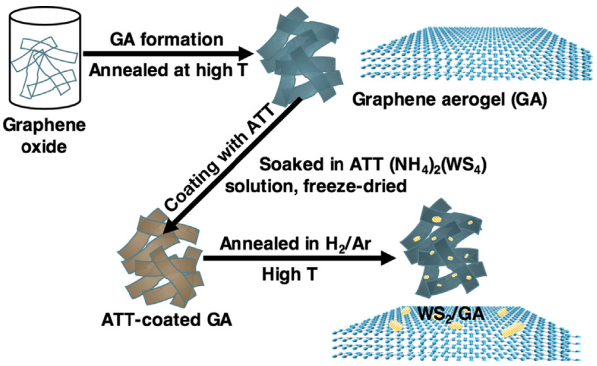

Fig. 1. Schematic illustration of the synthesis process for WS_2/graphene hybrid aerogel.

2.2. Sensor fabrication and sensing testing

The WS_2/GA is sonicated into suspension in isopropyl alcohol (0.5 mg/mL). A 1 μL drop (five drops of 0.2 μL each) is placed onto a sensor electrode device, while heating the chip at 100 °C for 3 h on a hotplate to promote solvent evaporation and material deposition at the center of the electrode chip. The schematic diagram of the conductometric gas sensor is shown in Fig. 2a.

For sensor testing, the device is placed in a stainless steel gas flow chamber (~13 cm^3 volume). Gas exposure and signal collection are controlled using Labview and an open-source Java-based instrument and control and measurement software suite, Zephyr. Gas tanks of NO_2 (Praxair, 20 ppm in N_2) are controlled with mass flow controllers (Bronkhurst) and mixed with an appropriate amount of water vapor and air to yield the desired gas concentration and relative humidity with a total flow rate of 300 sccm. For sensor signal collection, a bias voltage is applied to the sensor and the sensor's resistance is measured with a Keithley 2602A source-meter. The temperature of the sensing environment is controlled by heating the sensor chamber using resistive heating.

3. Results and discussion

3.1. Characterization

Raman spectrum of WS_2/GA in Fig. 2b confirms the presence of WS_2 and graphene. The main peaks found for WS_2 are A_{1g} (419 cm^{-1}) and E_{2g} (353 cm^{-1}). The peak position for the A_{1g} mode, which is the strongest indicator of coupling between layers, is consistent with literature reports for few-layered WS_2 [25,26]. The Raman peaks associated with carbon for WS_2/GA are very similar to those of graphene aerogel with strong, broad D (1328 cm^{-1}) and G (1588 cm^{-1}) bands and weak, poorly defined D' (1615 cm^{-1}) and 2D (2651 cm^{-1}) bands [21]. The 2D/G band intensity ratio and the position of the 2D band indicate the number of layers and stacking sequences [27]. The hybrid aerogel has a 2D/G band intensity ratio ~1, and a single, broad 2D peak with a large upshift compared to monolayer graphene, indicating few-layer turbostratic graphene [27]. A weak D + D′ peak (2932 cm^{-1}) demonstrates the disordered structure of graphene [28].

Electron microscopy gives more insight into how the WS_2 and graphene are assembled in the hybrid material. SEM images of this hybrid material deposited on the sensor device (Fig. 2c and d) show that the material is made of a continuous 3D assembly of interconnected nanosheets, which is consistent with the microstructure of this material before deposition (Fig. S1, Supporting Information). Additionally, this morphology is very similar to that exhibited by the graphene aerogel control sample (Fig. S2). Low-resolution TEM of the hybrid aerogel shows the WS_2 coating on graphene aerogel (Fig. 2e). In high-resolution TEM analysis as shown in Fig. 2f and g, graphene and WS_2 can be distinguished from their lattice spacing (3.5 Å vs 6.1 Å, respectively), indicating the graphene in one to six-layer sheets and WS_2 in one to five-layer sheets. These results support the Raman spectra (Fig. 2b). Therefore, the layered nature of the 2D materials are preserved in the 3D aerogel structure.

The XRD pattern in Fig. 3a further confirms the crystalline nature of WS_2/GA, showing the characteristic peaks for hexagonal graphene (JCPDS-ICDD 89-8487) and WS_2 (JCPDS-ICDD 87-2417). The

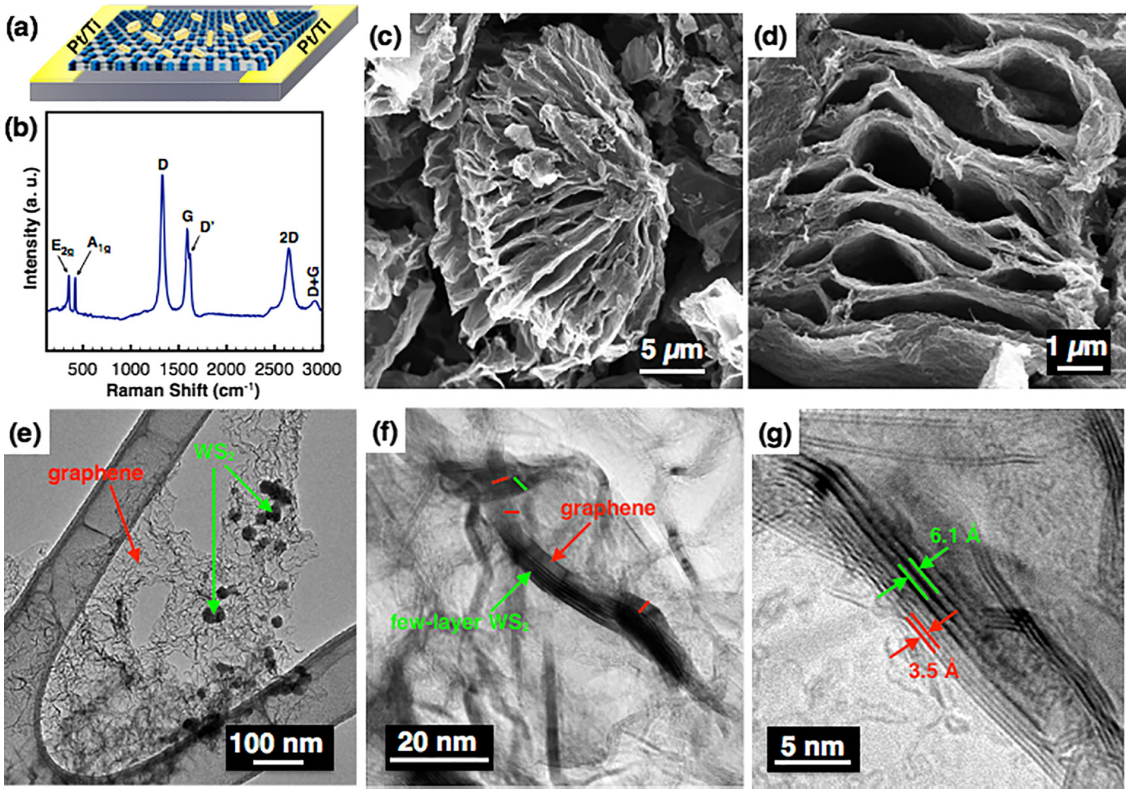

Fig. 2. (a) Schematic diagram of the resistive WS_2/GA-based sensor. (b) Raman spectrum of WS_2/GA. (c, d) SEM images of WS_2/GA on sensor device. TEM images of the as-prepared WS_2/GA: (e) low magnification image, (f, g) high resolution images, showing the graphene is coated by few-layer WS_2.

(002) peak of WS_2 at ~16°, as well as the strong (002) peak of graphene at ~26° suggests turbostratic stacked sheets in the aerogel [29].

Nitrogen porosimetry was used to characterize the textural properties of the hybrid aerogel. The nitrogen adsorption/desorption isotherm for the hybrid aerogel exhibits the Type 3 hysteresis loop (IUPAC classification) at relatively high pressure (Fig. 3b), which is typically associated with adsorption within aggregates of plate-like particles, consistent with the morphology observed in the SEM and TEM images (Fig. 2). Pore size distribution shows a bimodal distribution with peaks at 4 and 40 nm for the hybrid aerogel, with most of the surface area in the 4 nm range. The BET surface area is 102 m^2/g, which is much larger than the values reported for other nanostructured WS_2 [30,31] and is made possible by the graphene scaffold as shown *via* TEM (Fig. 2e–g), as well as by the large native surface area of the graphene aerogel [30].

X-ray photoelectron spectroscopy was performed to determine the composition and chemical states of the various species in the aerogel. The XPS survey spectrum of WS_2/GA demonstrates the coexistence of W, S and C (Fig. S3, Supporting Information). According to XPS analysis (Fig. 3c–e), W 4f signal in the aerogel is due to W(IV) species in WS_2 (W $4f_{7/2}$, BE = 32.5 eV), S 2p is due to S^{2-} (S $2p_{3/2}$, BE = 162.0 eV), C is due to C 1 s (BE = 284.1 eV). The relative atomic concentration of W, S, C is 9.1, 19.3 and 71.6% respectively. This suggests there is no bonded oxygen in the aerogel. The sulfur to tungsten ratio is calculated to be 2.11, slightly S-rich.

3.2. Gas sensing performances

Nearly linear current vs. voltage behavior of the WS_2/GA-based sensor both in RT and 180 °C dry atmosphere suggests an Ohmic contact between WS_2/GA and sensor electrodes (Fig. 4). It also shows a decreasing resistance in higher temperature (180 °C), consistent with the typical behavior of semiconductors. An Ohmic contact is also formed in the control GA-based sensor (Supporting Information, Fig. S3).

We investigated the sensing performance of the device in terms of percentage response, response time, percentage recovery and recovery time. Percentage response is defined by the percentile resistance change when the sensor is exposed to an analyte gas as follows:

$$Response = \frac{R_0 - R_g}{R_0} \times 100\% \quad (1)$$

where R_0 and R_g are the resistances of the sensor before and after exposure to the analyte gas, respectively. Percentage recovery is evaluated as follows:

$$Recovery = \frac{R_a - R_g}{R_0 - R_g} \times 100\% \quad (2)$$

where R_a is the resistance of the sensor exposed to air for a given recovery time. The response time ($t_{response}$) is defined as the time taken to reach 90% of the full response after the introduction of the target gas. The recovery time ($t_{recovery}$) is defined as the time taken to return to 90% of the baseline resistance after the flow of target gas is stopped.

Fig. 5(a) shows the effect of ambient temperature on the response to 2 ppm NO_2 of 10 min duration. The ambient temperature was varied from 20 to 180 °C. There is a clear trend from higher response and slow response/recovery rate in 20 °C atmosphere to lower response and faster response/recovery rate under higher ambient temperature. The recovery increases from 25% to 100% gradually with the ambient temperature increasing from 20

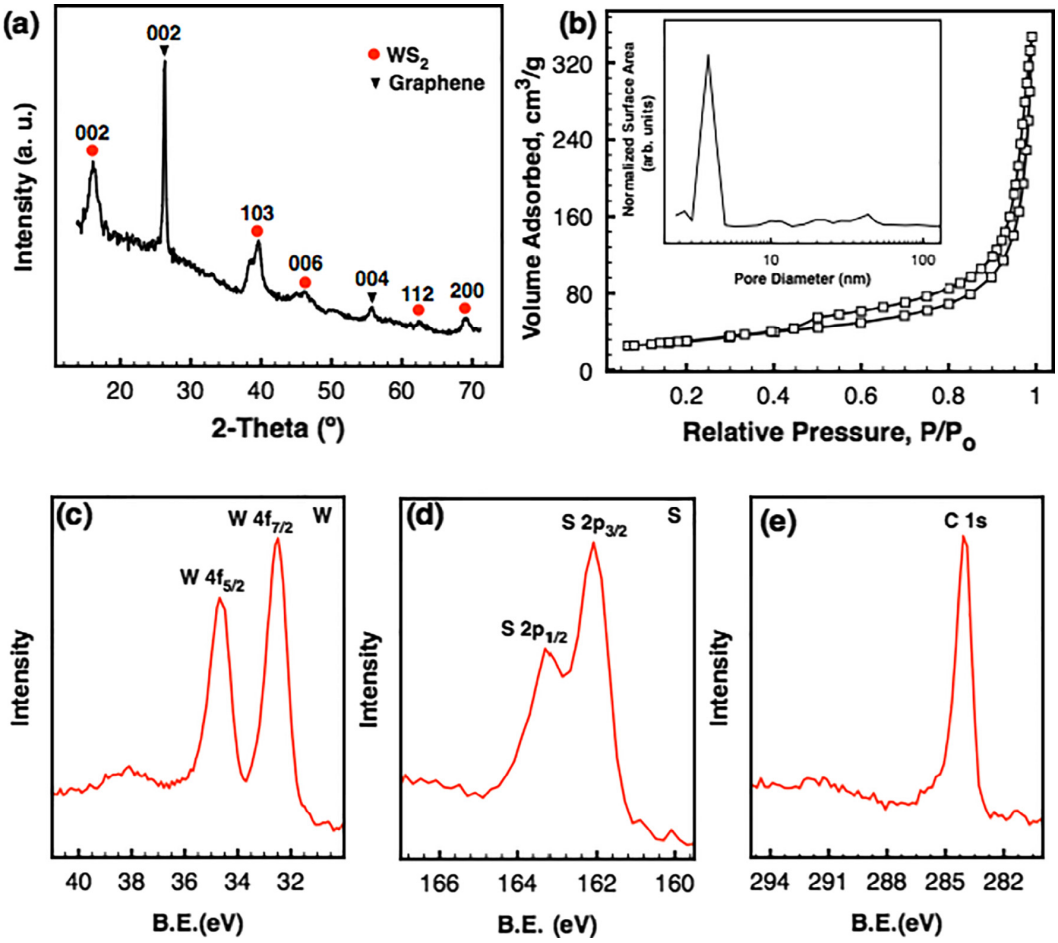

Fig. 3. (a) XRD and (b) Nitrogen adsorption/desorption isotherms for WS_2/GA. Inset of (b) shows pore size distribution for the hybrid aerogel. XPS spectra of (c) W 4f, (d) S 2p and (e) C 1s regions in WS_2/GA.

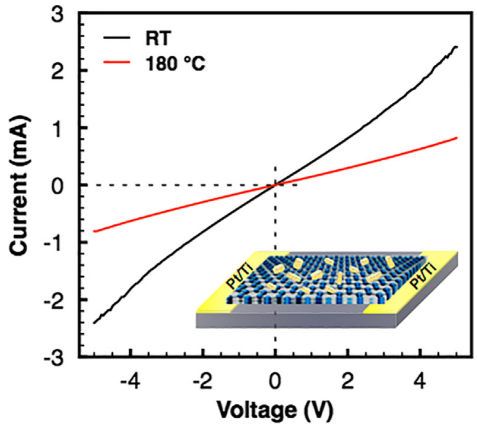

Fig. 4. Linear I/V plots of the WS_2/GA-based sensor in dry environment of RT and 180 °C.

to 180 °C, while the response decreases from 6.5% to 3%. This behavior is consistent with the following sensing mechanism. At low temperatures, the adsorption of NO_2 is substantial during the gas exposure, while the desorption is weak due the strong bonding between NO_2 and WS_2/GA. Thus, the equilibrium between adsorption and desorption is not reached within the probed timeframe. With increasing temperature, the rate of NO_2 desorption is increased, allowing a balance between adsorption and desorption to be reached more rapidly during gas exposure and afterwards during the recovery step.

The most remarkable benefit of WS_2/GA composite is the improved selectivity to NO_2, compared to the control WS_2 aerogel and GA samples. As reported in our previous work [32], the WS_2 aerogel sensor responds to NO_2, H_2, NH_3, and O_2 gases with poor selectivity in dry air. As shown in Fig. 6a, the GA sensor responds to H_2, NH_3 and NO_2, with the highest response percentage to 2000 ppm H_2 at 180 °C. In contrast, the WS_2/GA sensor shows excellent selectivity to NO_2 at much lower concentration (2 ppm), with a weak response to H_2 and NH_3 at much higher concentration level (2000 and 200 ppm, respectively). Additionally, for both GA control sample and WS_2/GA, the resistance of the sensors increases when exposure to reducing gases (such as H_2 and NH_3), and decreases when exposure to oxidizing gases (for example, NO_2).

The enhancement of selectivity is attributed to the following processes. According to the previous work, both graphene [14] and WS_2 aerogel [32] exhibit p-type behavior. Based on the energy level diagram for graphene and WS_2, similar to the reported one for MoS_2/graphene heterostructures [33], a potential barrier (Φ) is

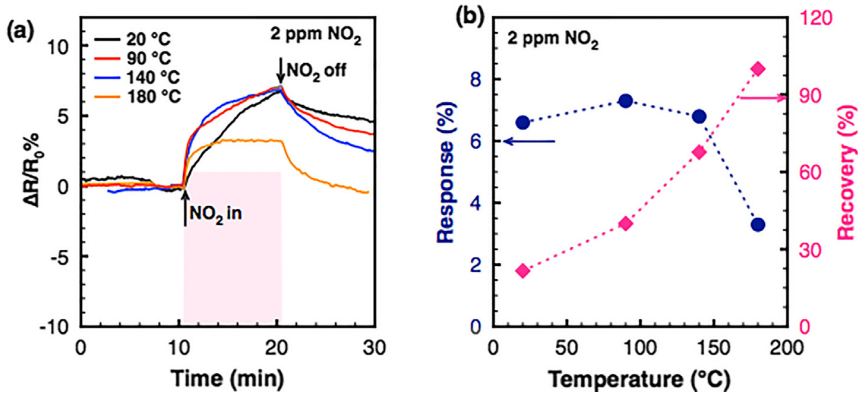

Fig. 5. (a) Response of the WS_2/GA-based sensor to 2 ppm NO_2 in dry environment at different ambient temperatures. (b) Response and recovery percentage of the WS_2/GA-based sensor vs. ambient temperature to 2 ppm NO_2 in dry air, showing decreasing response and increasing recovery percentage with temperature.

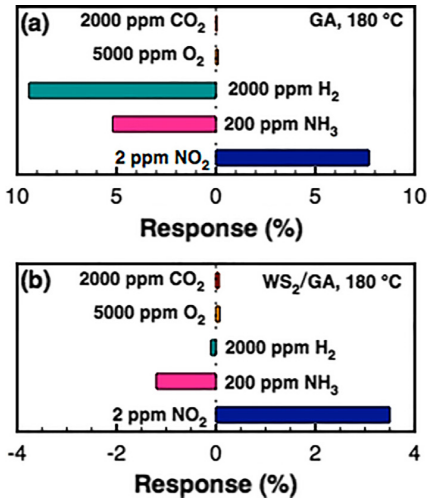

Fig. 6. Selectivity of the WS_2/GA sensor compared to the underlying GA sensor in 180 °C dry atmosphere.

formed due to the work function difference between graphene and WS_2 (Fig. 7a). When exposure to NO_2, NO_2 molecules capture electrons of the sensing aerogel (Fig. 7b), decreasing the junction barrier height. When exposure to reducing gases (e.g. NH_3, Fig. 7b), the reducing gas molecules contribute electrons to the sensing aerogel increasing the junction barrier height, which adversely affects the charge transfer between aerogel and analyte gas. Furthermore, as the NO_2 has a higher electron affinity, WS_2 coating improves the response to NO_2, but suppresses the response to NH_3 and H_2. NO_2 adsorption on WS_2/GA and the sensing mechanism agree well with the previous reports on WS_2 functionalized carbon nanofibers [34], ZnO/graphene aerogel [15] and rGO-Cu_2O [35] composite-based gas sensors.

The effect of repeated exposure of the sensor to 2 ppm NO_2 at RT under different RH atmospheres is shown in Fig. 8(a). The resistance of the sensor decreases upon exposure to NO_2, consistent with p-type behavior, according to the following Eq. (3):

$$NO_2 + e^- \Longleftrightarrow NO_2^- \quad (3)$$

After the sensor is exposed to 2 ppm NO_2 for 3 sensing cycles, the response decreases by about 71% in dry air, the response is stable in 30% RH atmosphere, and the response decreases by about 16% in 60% RH atmosphere (Fig. 8b). The recovery is incomplete in dry air after exposed to air during the given recovery time of 10 min, but complete recovery in both 30% and 60% RH atmosphere is achieved in this timeframe (Fig. 8a). Hence, humidity enhances the response and recovery behavior of the WS_2/GA sensor to NO_2 at RT, which is consistent with the sensing behavior of bottom-gate graphene FET sensors [18]. Both under 30% and 60% RH conditions at RT, the response time to 2 ppm NO_2 is around 70 s, while the recovery time is around 300 s. Moreover, as shown in Fig. 8a, the resistance of the WS_2/GA sensor decreases with the ambient humidity increasing.

The resistance change of the WS_2/GA at room temperature is associated with the movement of the proton $H^{\pm}$ or $H_3O^{\pm}$ within the physisorbed water because of the Grotthus transport mechanism [36–39]. The physisorption of water molecules takes place below 100 °C. As humidity levels increase at room temperature, the protons migrate more easily resulting in decreased resistance of WS_2/GA, and lower junction barrier. As well, based on Eqs. (3) and (4)

$$NO_2^- + H^+ \Longleftrightarrow HNO_2 \quad (4)$$

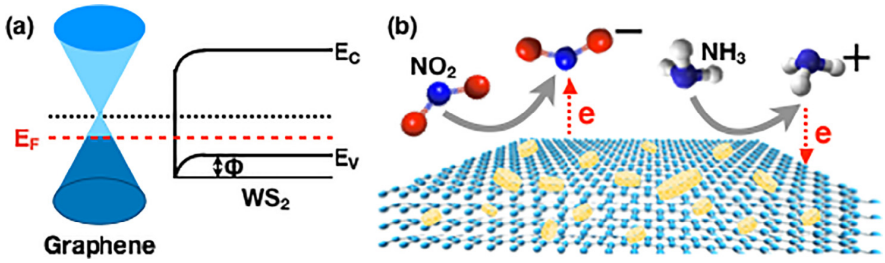

Fig. 7. Gas sensing mechanism of the WS_2/GA heterojunction. (a) Proposed band diagram. (b) Electrons transfer between the analyte gases and WS_2/GA.

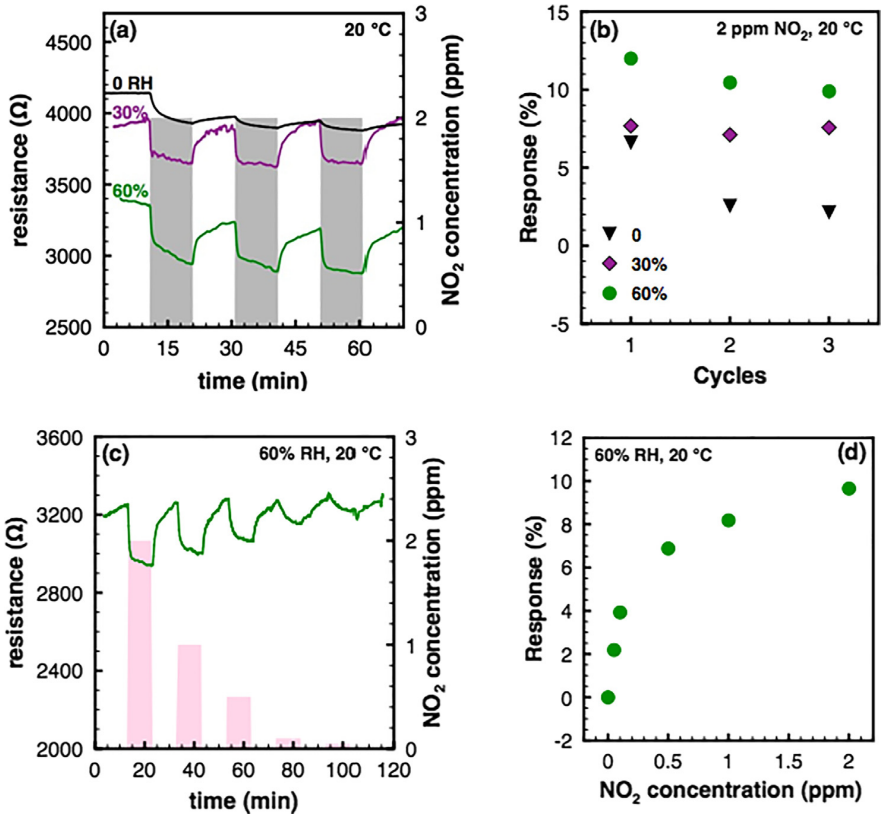

Fig. 8. (a) Resistance change of the WS_2/GA sensor with cyclic exposures, (b) Percentage response during the sensing cycles to 2 ppm NO_2 at RT under different RH atmospheres. (c) Real time response and (d) response *vs.* NO_2 concentration of the WS_2/GA sensor to different NO_2 concentrations at RT under 60% RH atmosphere.

high humidity is beneficial to NO_2 adsorption. Therefore, humidity is found helpful for enhancing the response and recovery of the composite aerogel to NO_2.

The real-time response of the WS_2/GA sensor to NO_2 of varied concentrations from 0.05 to 2 ppm at RT under 60% RH atmosphere is shown Fig. 8c. The response *vs.* NO_2 concentration shows the response increasing monotonically with NO_2 concentration (Fig. 8d). A practical limit for gas sensor requires a signal-to-noise ratio (SNR) of at least 3. Thus, the theoretical detection limit is around 10 ppb (SNR = 3), which is comparable to or lower than previous reports on high-performance NO_2 sensors such as graphene/MoS_2 (41.4 ppb) [40].

The WS/GA sensor does not exhibit any obvious changes in its response to NO_2 at 180 °C under different humidity conditions, for example, as shown in Fig. 9a, for the percentage response to 2 ppm NO_2. Additionally, the response time is around 100 s, while the recovery time around 300 s to 2 ppm NO_2 in all the conditions. The resistance *vs.* time of the WS_2/GA sensor to different NO_2 concentrations in 180 °C dry ambient is shown in Fig. S5(a) (Supporting Information). Because of the weak OH-binding forces at higher temperature [41], NO_2 sensing performances remain stable at 180 °C under different humidity environments. The resistance *vs.* time of the WS_2/GA sensor when exposed to NO_2 with varied concentrations (0.05–2 ppm) at 180 °C in 60% RH atmosphere is shown

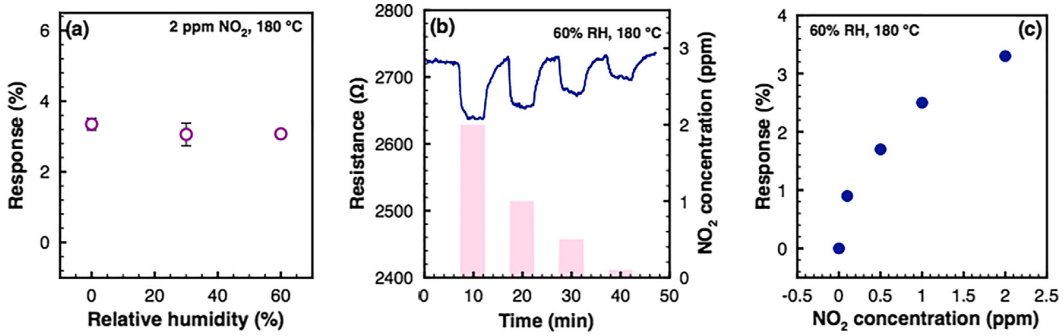

Fig. 9. (a) Percentage response to 2 ppm NO_2 at 180 °C under different RH atmospheres. The error bars represent the standard deviation of response of the 3 exposures to 2 ppm NO_2. (b) Real time response and (c) response *vs.* NO_2 concentration of the WS_2/GA sensor to different NO_2 concentrations at 180 °C under 60% RH atmosphere.

Fig. 9b. Fig. 9c shows the response of the WS_2/GA sensor increasing monotonically with NO_2 concentration. Based on the data, the detection limit, corresponding to signal-to-noise ratio of 3 is 15 ppb.

4. Conclusions

We report on the effects of ambient humidity and temperature on the NO_2 sensing performance of the WS_2/graphene composite aerogel-based conductometric sensor. At room temperature, the NO_2 sensing behavior, including response and recovery, is improved with increased humidity level of the environment. In dry atmosphere, by increasing the temperature to 180 °C, the response to and recovery rates of NO_2 increase, and the signal recovery is enhanced, but the signal response decreases. At a temperature of 180 °C, the NO_2 sensing performance of the hybrid sensor remains stable over a wide humidity range (0–60%). The hybrid aerogel sensor shows excellent selectivity to NO_2 with the detection limit of 10–15 ppb. This work indicates the potential of WS_2/-graphene aerogel for the detection of NO_2 outdoors, specifically for the screening of atmospheric quality in a range of practical daily conditions.

Acknowledgements

The authors acknowledge Steven Delacruz for help with the SEM analysis. This work was supported by Berkeley Sensor & Actuator Center (BSAC) Industrial Members and National Science Foundation (NSF Grant No. IIP 1444950), which provided for the design of experiments, student support (W.Y) and sensor fabrication and performance characterization. T.P. and A.Z. acknowledge the Air Force Office of Scientific Research under contract FA9550-14-1-0323, which provided for student support (T.P.) and instrumentation; and the Director, Office of Science, Office of Basic Energy Sciences, Materials Science and Engineering Division, of the U.S. Department of Energy under contract no. DE-AC02-05CH11231 within the sp^2-bonded Materials Program (KC2207), which provided for TEM characterization. M.W. would like to acknowledge the support of Lawrence Livermore National Laboratory under the auspices of the U.S. Department of Energy under Contract DE-AC52-07NA27344, through LDRD award 13-LW-099. W.Y. acknowledge additional support through the China Scholarship Council.

Appendix A. Supplementary material

Supplementary data associated with this article can be found, in the online version, at https://doi.org/10.1016/j.apsusc.2018.04.185.

References

[1] A. Stănoiu, C. Simion, L. Diamandescu, D. Tărăbăşanu-Mihăilă, M. Feder, NO_2 sensing properties of Cr_2O_3 highlighted by work function investigations, Thin Solid Films 522 (2012) 395–400.
[2] A. Stănoiu, C. Simion, S. Somăcescu, NO_2 sensing mechanism of ZnO–Eu_2O_3 binary oxide under humid air conditions, Sensors Actuators B: Chem. 186 (2013) 687–694.
[3] X. Pan, X. Zhao, A. Bermak, Z. Fan, A humidity-insensitive NO_2 gas sensor with high selectivity, IEEE Electron Dev. Lett. 37 (2016) 92–95.
[4] J.-S. Kim, J.-W. Yoon, Y.J. Hong, Y.C. Kang, F. Abdel-Hady, A. Wazzan, J.-H. Lee, Highly sensitive and selective detection of ppb-level NO_2 using multi-shelled WO_3 yolk–shell spheres, Sens. Actuators, B 229 (2016) 561–569.
[5] F. Liu, B. Wang, X. Yang, Y. Guan, Q. Wang, X. Liang, P. Sun, Y. Wang, G. Lu, High-temperature NO_2 gas sensor based on stabilized zirconia and $CoTa_2O_6$ sensing electrode, Sens. Actuators, B 240 (2017) 148–157.
[6] F. Liu, B. Wang, X. Yang, Y. Guan, R. Sun, Q. Wang, X. Liang, P. Sun, G. Lu, High-temperature stabilized zirconia-based sensors utilizing MNb_2O_6 (M: Co, Ni and Zn) sensing electrodes for detection of NO_2, Sens. Actuators, B 232 (2016) 523–530.
[7] Z. Ling, C. Leach, The effect of relative humidity on the NO_2 sensitivity of a SnO_2/WO_3 heterojunction gas sensor, Sens. Actuator B-Chem. 102 (2004) 102–106.
[8] Y.W. Zhu, S. Murali, W.W. Cai, X.S. Li, J.W. Suk, J.R. Potts, R.S. Ruoff, Graphene and graphene oxide: synthesis, properties, and applications, Adv. Mater. 22 (2010) 3906–3924.
[9] M. Chhowalla, H.S. Shin, G. Eda, L.J. Li, K.P. Loh, H. Zhang, The chemistry of two-dimensional layered transition metal dichalcogenide nanosheets, Nat. Chem. 5 (2013) 263–275.
[10] K.Y. Ko, J.G. Song, Y. Kim, T. Choi, S. Shin, C.W. Lee, K. Lee, J. Koo, H. Lee, J. Kim, T. Lee, J. Park, H. Kim, Improvement of gas-sensing performance of large-area tungsten disulfide nanosheets by surface functionalization, ACS Nano 10 (2016) 9287–9296.
[11] N.J. Huo, S.X. Yang, Z.M. Wei, S.S. Li, J.B. Xia, J.B. Li, Photoresponsive and gas sensing field-effect transistors based on multilayer WS_2 nanoflakes, Sci. Rep. 4 (2014) 9.
[12] R.A. Potyrailo, C. Surman, N. Nagraj, A. Burns, Materials and transducers toward selective wireless gas sensing, Chem. Rev. 111 (2011) 7315–7354.
[13] J.D. Fowler, M.J. Allen, V.C. Tung, Y. Yang, R.B. Kaner, B.H. Weiller, Practical chemical sensors from chemically derived graphene, Acs Nano 3 (2009) 301–306.
[14] F. Schedin, A.K. Geim, S.V. Morozov, E.W. Hill, P. Blake, M.I. Katsnelson, K.S. Novoselov, Detection of individual gas molecules adsorbed on graphene, Nat. Mater. 6 (2007) 652–655.
[15] X. Liu, J.B. Sun, X.T. Zhang, Novel 3D graphene aerogel-ZnO composites as efficient detection for NO_2 at room temperature, Sens. Actuator B-Chem. 211 (2015) 220–226.
[16] F.L. Meng, Z. Guo, X.J. Huang, Graphene-based hybrids for chemiresistive gas sensors, Trac-Trends Anal. Chem. 68 (2015) 37–47.
[17] H. Choi, J.S. Choi, J.S. Kim, J.H. Choe, K.H. Chung, J.W. Shin, J.T. Kim, D.H. Youn, K.C. Kim, J.I. Lee, S.Y. Choi, P. Kim, C.G. Choi, Y.J. Yu, Flexible and transparent gas molecule sensor integrated with sensing and heating graphene layers, Small 10 (2014) 3685–3691.
[18] C.H. Kim, S.W. Yoo, D.W. Nam, S. Seo, J.H. Lee, Effect of temperature and humidity on NO_2 and NH_3 gas sensitivity of bottom-gate graphene FETs prepared by ICP-CVD, IEEE Electron Dev. Lett. 33 (2012) 1084–1086.
[19] B. Alfano, T. Polichetti, M.L. Miglietta, E. Massera, C. Schiattarella, F. Ricciardella, G. Di Francia, Fully eco-friendly H_2 sensing device based on Pd-decorated graphene, Sens. Actuators, B 239 (2017) 1144–1152.
[20] F. Rigoni, R. Maiti, C. Baratto, M. Donarelli, J. MacLeod, B. Gupta, M. Lyu, A. Ponzoni, G. Sberveglieri, N. Motta, Transfer of CVD-grown graphene for room temperature gas sensors, Nanotechnology (2017).
[21] M.A. Worsley, T.T. Pham, A.M. Yan, S.J. Shin, J.R.I. Lee, M. Bagge-Hansen, W. Mickelson, A. Zettl, Synthesis and characterization of highly crystalline graphene aerogels, Acs Nano 8 (2014) 11013–11022.
[22] M.A. Worsley, S.O. Kucheyev, H.E. Mason, M.D. Merrill, B.P. Mayer, J. Lewicki, C. A. Valdez, M.E. Suss, M. Stadermann, P.J. Pauzauskie, J.H. Satcher, J. Biener, T.F. Baumann, Mechanically robust 3D graphene macroassembly with high surface area, Chem. Commun. 48 (2012) 8428–8430.
[23] M.A. Worsley, P.J. Pauzauskie, T.Y. Olson, J. Biener, J.H. Satcher, T.F. Baumann, Synthesis of graphene aerogel with high electrical conductivity, J. Am. Chem. Soc. 132 (2010) 14067–14069.
[24] J.L. Mohanan, I.U. Arachchige, S.L. Brock, Porous semiconductor chalcogenide aerogels, Science 307 (2005) 397–400.
[25] A. Berkdemir, H.R. Gutiérrez, A.R. Botello-Méndez, N. Perea-López, A.L. Elías, C.-I. Chia, B. Wang, V.H. Crespi, F. López-Urías, J.-C. Charlier, Identification of individual and few layers of WS_2 using Raman Spectroscopy, Sci. Rep. 3 (2013).
[26] H.L. Zeng, G.B. Liu, J.F. Dai, Y.J. Yan, B.R. Zhu, R.C. He, L. Xie, S.J. Xu, X.H. Chen, W. Yao, X.D. Cui, Optical signature of symmetry variations and spin-valley coupling in atomically thin tungsten dichalcogenides, Sci. Rep. 3 (2013).
[27] A.C. Ferrari, J.C. Meyer, V. Scardaci, C. Casiraghi, M. Lazzeri, F. Mauri, S. Piscanec, D. Jiang, K.S. Novoselov, S. Roth, A.K. Geim, Raman spectrum of graphene and graphene layers, Phys. Rev. Lett. 97 (2006).
[28] A. Eckmann, A. Felten, A. Mishchenko, L. Britnell, R. Krupke, K.S. Novoselov, C. Casiraghi, Probing the nature of defects in graphene by Raman spectroscopy, Nano Lett. 12 (2012) 3925–3930.
[29] G. An, C. Lu, C. Xiong, Solid-phase reaction synthesis of mesostructured tungsten disulfide material with a high specific surface area, Mater. Res. Bull. 46 (2011) 1323–1326.
[30] M.A. Worsley, S.J. Shin, M.D. Merrill, J. Lenhardt, A.J. Nelson, L.Y. Woo, A.E. Gash, T.F. Baumann, C.A. Orme, Ultralow density, monolithic WS_2, MoS_2, and MoS_2/graphene aerogels, ACS Nano 9 (2015) 4698–4705.
[31] X. Fang, C. Hua, C. Wu, X. Wang, L. Shen, Q. Kong, J. Wang, Y. Hu, Z. Wang, L. Chen, Synthesis and electrochemical performance of graphene-like WS_2, Chem.-Eur. J. 19 (2013) 5694–5700.
[32] W. Yan, A. Harley-Trochimczyk, H. Long, L. Chan, T. Pham, M. Hu, Y. Qin, Conductometric gas sensing behavior of WS_2 aerogel, FlatChem 5 (2017) 1–8.
[33] P. Vabbina, N. Choudhary, A.A. Chowdhury, R. Sinha, M. Karabiyik, S. Das, W. Choi, N. Pala, Highly sensitive wide bandwidth photodetector based on internal photoemission in CVD grown p-type MoS_2/graphene Schottky junction, ACS Appl. Mater. Interfaces 7 (2015) 15206–15213.
[34] J.H. Cha, S.J. Choi, S. Yu, I.D. Kim, 2D WS_2-edge functionalized multi-channel carbon nanofibers: effect of WS_2 edge-abundant structure on room temperature NO_2 sensing, J. Mater. Chem. A 5 (2017) 8725–8732.

[35] S. Deng, V. Tjoa, H.M. Fan, H.R. Tan, D.C. Sayle, M. Olivo, S. Mhaisalkar, J. Wei, C. H. Sow, Reduced graphene oxide conjugated Cu_2O nanowire mesocrystals for high-performance NO_2 gas sensor, J. Am. Chem. Soc. 134 (2012) 4905–4917.
[36] Z.Y. Wang, Y. Xiao, X.B. Cui, P.F. Cheng, B. Wang, Y. Gao, X.W. Li, T.L. Yang, T. Zhang, G.Y. Lu, Humidity-sensing properties of urchin like CuO nanostructures modified by reduced graphene oxide, ACS Appl. Mater. Interfaces 6 (2014) 3888–3895.
[37] Y.H. Tan, K. Yu, T. Yang, Q.F. Zhang, W.T. Cong, H.H. Yin, Z.L. Zhang, Y.W. Chen, Z.Q. Zhu, The combinations of hollow MoS_2 micro@nano-spheres: one-step synthesis, excellent photocatalytic and humidity sensing properties, J. Mater. Chem. C 2 (2014) 5422–5430.
[38] X.F. Wang, Y.P. Chen, H.W. Qin, L. Li, C.M. Shi, L. Liu, J.F. Hu, CO_2 sensing of $La_{0.875}Ca_{0.125}FeO_3$ in wet vapor: a comparison of experimental results and first-principles calculations, Phys. Chem. Chem. Phys. 17 (2015) 13733–13742.
[39] F. Pourfayaz, Y. Mortazavi, A. Khodadadi, S. Ajami, Ceria-doped SnO_2 sensor highly selective to ethanol in humid air, Sens. Actuator B-Chem. 130 (2008) 625–629.
[40] Y. Niu, W.C. Jiao, R.G. Wang, G.M. Ding, Y.F. Huang, Hybrid nanostructures combining graphene-MoS_2 quantum dots for gas sensing, J. Mater. Chem. A 4 (2016) 8198–8203.
[41] U. Hoefer, J. Frank, M. Fleischer, High temperature Ga_2O_3-gas sensors and SnO_2-gas sensors: a comparison, Sens. Actuator B-Chem. 78 (2001) 6–11.